Laser diffraction spectrometry : Fraunhofer diffraction versus Mie scattering

Laser Diffraction Spectrometry: Fraunhofer Diffraction Versus Mie Scattering

Gerben B. J. de Boer*, Cornelis de Weerd*, Dirk Thoenes*, Hendrik W. J. Goossens**

(Received: 21 October 1986)

Abstract

Laser diffraction spectrometry (LDS) is often claimed to operate on the principle of Fraunhofer diffraction. This is only true, however, if particles are large compared to the wavelength of light or if the ratio of the refractive indices of the disperse and continuous phases, m, is clearly different from unity. In this study it has been established that LDS, as applied to particle and droplet sizing in suspensions and emulsions, is based on Mie-scattering. Scattering patterns of single particles may be calculated if the refractive indices of both phases are known. Thus, a theoretical basis has been provided for the application of LDS to size-measurement in suspensions and emulsions, and for extension of this method to the lower size ranges and those cases in which the refractive indices of the disperse and continuous phases are similar. Extension of the work presented in this paper will enable the calculation of scattering matrices so that calibration of the apparatus with standard materials may be avoided.

1 Introduction

One of the latest techniques in droplet- and particle-sizing is laser diffraction spectrometry (LDS). Unlike other optical techniques, LDS does not require single particles to be measured successively, in order to obtain a size distribution (SD). Instead, interaction between light and the ensemble of all illuminated particles is analysed. Analysis is rapid and makes on-line measurements possible. Change of sample, sample preparation and analysis time can be reduced to a minimum. This technique therefore, is particularly useful in studying aggregation and dispersion phenomena.

The theory, describing the interaction between small particles and light is called Lorenz-Mie theory [1]. It starts from Maxwell's equations for an electromagnetic field and results in an exact description of the field when an interaction takes place. If the particles are large relative to the wavelength of the light, the interaction may be interpreted in terms of diffraction. Further, if the distances of the light-source and detection plane from the point of intersection of the scattering object, are large compared to the wavelength of light, the interaction is described by Fraunhofer diffraction theory (FD).

An increasing number of commercial versions of the apparatus are claimed to operate on the principle of FD, a limiting case of Lorenz-Mie theory. This view is generally accepted by other workers in the field of particle sizing, and supported by both experimental and theoretical studies [2-6]. However, most of this work is concerned with the measurement of solids or of sprays suspended in a gas where the refractive indices of continuous and dispersed phases differ appreciably. When particles suspended in a liquid are analysed, the application of FD theory is questionable, in particular if the particles are small compared to the wavelength of light and the refractive indices are similar. This work was aimed at finding the basic principles of LDS as applied to the sizing of particles in suspension, so as to acquire a clear picture of the measuring process and to define its limitations. The study was carried out as part of a research program on aggregation phenomena in turbulent liquid flows.

2 Principles of Measurement

To obtain a better understanding of LDS, the principles of measurement will be briefly described.

Figure 1 shows two spherical particles of equal size which are exposed to a coherent beam of parallel monochromatic light. Light, scattered at equal angles is also parallel and is, therefore, focussed onto one specific point in the detection plane by a lens. This image point, combined with those corresponding to light scattered at other angles, creates the far-field scattering pattern of the particles. This pattern is neither affected by the position of the particles in the beam nor by their state of motion.

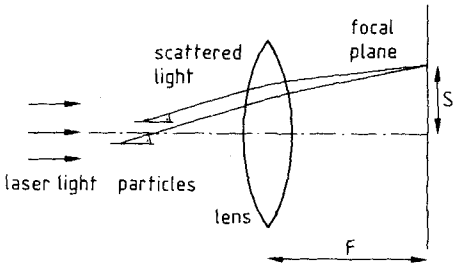

Fig. 1: Two spherical particles of equal size which are exposed to a coherent beam of parallel monochromatic light.

* *G. B. J. de Boer,* M. Sc., *C. de Weerd,* M. Sc., Prof. *D. Thoenes,* Ph. D., M. Sc., Eindhoven University of Technology, Department of Chemical Engineering, Eindhoven, 5612 AZ (The Netherlands).

** *H. W. J. Goossens,* M. Sc., Philips Product Development Division, Eindhoven (The Netherlands).

0176-2265/87/0103-0014 $02.50/0

Assume, for reasons of simplicity, that the interaction between particles and light is described by FD theory. The diffraction pattern is then only dependent on particle size. Let the parameter, x, be defined by:

$$x = \frac{2\pi rs}{\lambda F} . \tag{1}$$

Figure 2 presents the diffraction pattern in a form, which is valid for all particle diameters. Light intensity is plotted as a function of the radial distance from the centre of the focal plane of the lens. This pattern is rotationally symmetrical.

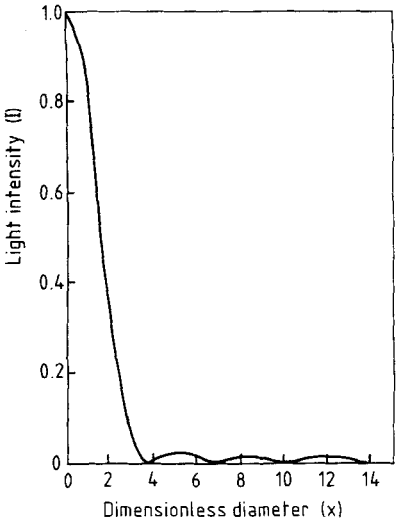

Fig. 2: Intensity distribution for the case of Fraunhofer diffraction for a circular disk or aperture.

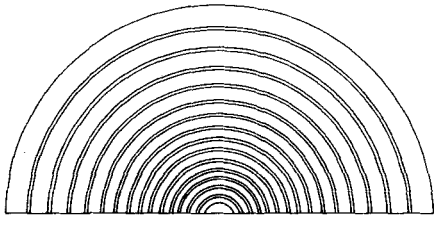

Fig. 3: Schematic of detector that consists of a series of concentric photosensitive rings separated by insulating gaps.

Measuring the intensity pattern for the purpose of inferring a SD is rather difficult [6], analysing the light energy distributed over a finite area of the detector is more fruitful [7].
For the instrument to be described later, the detector consists of a series of concentric rings (see Figure 3). It can be shown that the energy (1) falling on the detector segment with radii s_1 and s_2 due to a particle of radius, r, is given by:

$$L_{s1,s2} = C\pi r^2 \{[J_0^2(x) + J_1^2(x)]_{s1} - [J_0^2(x) + J_1^2(x)]_{s2}\} . \tag{2}$$

Here, πr^2, the particle cross-sectional area, is proportional to the light energy falling on the particle; C is an optical constant which depends on the intensity of the incident light and efficiency of the optical arrangement.

For N particles of radius r, the appropriate expression is N times that given in Eq. (2). Therefore, the light energy falling on the detector ring, owing to a large number of particles of different sizes, is:

$$L_{s1,s2} = C\pi \sum_{i=1}^{M} N_i r_i^2 \{[J_0^2(x_i) + J_1^2(x_i)]_{s1} - [J_0^2(x_i) + J_1^2(x_i)]_{s2}\} \tag{3}$$

where the SD has been divided into M classes.
In practice it is convenient to work with weight distributions rather than with distributions based on particle numbers. Assuming the density of the particles to be independent of size, we may write:

$$W_i = 4/3\,\pi r_i^3 \rho N_i . \tag{4}$$

Using this relation, Eq. (3) may be transformed as follows:

$$L_{s1,s2} = K \sum_{i=1}^{m} \left(\frac{W_i}{r_i}\right) \{[J_0^2(x_i) + J_1^2(x_i)]_{s1} - [J_0^2(x_i) + J_1^2(x_i)]_{s2}\}$$

$$= \sum_{i=1}^{m} C_{i,s1-s2} W_i . \tag{5}$$

The same equation applies, of course, to the other detector elements. The instrument used in this study measures 15 increments on the energy distribution. Thus, 15 linear equations, similar to that expressed by Eq. (5), are obtained and the size distribution is supposed to consist of 15 classes. Once the distribution of light energy has been measured, this set may be solved, yielding the most likely distribution of particle size on a basis of weight.
The set of linear Eqs. (5) can also be expressed in matrix-notation:

$$\underline{L} = \underline{\underline{A}}\,\underline{W} . \tag{6}$$

The matrix $\underline{\underline{A}}$ is called the scattering matrix. Each of its elements, $a(ij)$, represents the specific light-energy falling onto detector segment, i, caused by particles within size-interval, j.
The analytical solution to this problem is:

$$\underline{W} = \underline{\underline{A}}^{-1}\,\underline{L} . \tag{7}$$

Numerical methods based on the principle of matrix inversion were worked out by *Heuer* and *Leschonski*[3].
A second method is that of function minimization. Starting from an estimated value for the actual weight distribution of the sample, $\underline{W}_{est}$, one may calculate the corresponding energy distribution, $\underline{L}_{est}$, by using Eq. (6). Let the object function, Q, be defined as:

$$Q = \sum_{k=1}^{M} [(L(k) - L_{est}(k))/s(k)]^2 \tag{8}$$

where $L(i)$ and $L_{est}(i)$ represent the light energies on detector segment i, as actually measured and estimated respectively. The term $s(i)$ represents a weighting factor. Minimization of the object function will lead to the most likely weight distribution of the particles of the dispersed phase which corresponds to the measured scattering pattern.

3 Optical Set-up

The measurement of scattering patterns was carried out by means of a Malvern 2600 HSLBD particle sizer. The optical arrangement is shown schematically in Figure 4.
A 2 – mW He – Ne, unpolarized laser beam is spatially filtered, expanded to 9 millimeters, and collimated. Particles are allowed to move across this beam. The scattered and transmitted light are focussed by a lens onto the detector, situated in the focal plane of the lens.

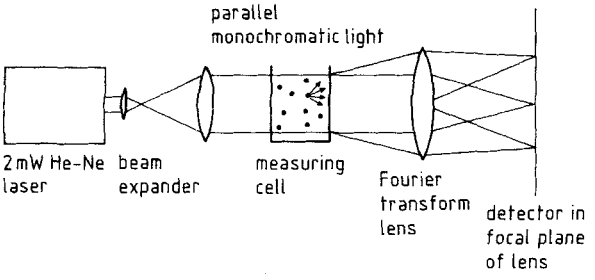

Fig. 4: Schematic of laser diffraction particle sizing instrument.

In this study, a lens with a focal length of 63 millimeters was used. The geometry of the detector is of special importance. This detector consists of semi-circular elements, as stated in the previous section. The radii of these elements are listed in Table 1.

Table 1: Dimensions of the annular detector elements of the Malvern 2600 HSLBD photodiode array detector.

Detector ring No.	Inner radius (mm)	Outer radius (mm)
1	0.149	0.218
2	0.254	0.318
3	0.353	0.417
4	0.452	0.518
5	0.554	0.625
6	0.660	0.737
7	0.772	0.856
8	0.892	0.986
9	1.021	1.128
10	1.163	1.285
11	1.321	1.461
12	1.496	1.656
13	1.692	1.880
14	1.915	2.131
15	2.167	2.416
16	2.451	2.738
17	2.774	3.101
18	3.137	3.513
19	3.549	3.978
20	4.013	4.501
21	4.536	5.085
22	5.121	5.738
23	5.773	6.469
24	6.505	7.282
25	7.318	8.184
26	8.219	9.185
27	9.220	10.287
28	10.323	11.501
29	11.537	12.837
30	12.873	14.300

The powders were suspended in liquid in a stirred measuring cell (Malvern, type PS 14). The pathlength of the light passing through this cell is 14.3 millimeters. The process of measurement was controlled by a microcomputer. An experiment was preceded by a measurement of the background which is subtracted from the time average signal. The signal from each successive pair of rings was added and averaged. Since the response of the detector rings to light-energy is not completely linear and the area of the different elements is different, the measurements are corrected by calibration factors. The data then represents the 15 L-values which appear in Eq. (5) and were used to compute the particle size distribution.

4 Results from Theory and Experiment

Understanding of the physical background for measuring particles or droplets in a liquid phase, lies in the prediction of the scattering patterns as recorded by the apparatus. Usually discrete size-intervals are used in LDS. The size-class limits of the weight distribution as used by the Malvern apparatus for the 63 millimeter focal length lens, are listed in Table 2. The scattering matrix for this lens which appears in the software of the instrument, is given in Table 3. The elements of columns 1 through 15 represent the scattering pattern of the size-classes given in Table 2 and are denoted by the same number. Adopting the same size-class limits and accounting for the optical set-up and detector geometry of the measuring apparatus, scattering patterns were calculated by us based on Lorenz-Mie theory [8] and the FD approach respectively.

Table 2: Size classes of Malvern 2600 HSLBD for a 63 mm lens.

Upper size class (micron)	Lower size class (micron)
118.4	54.9
54.9	33.7
33.7	23.7
23.7	17.7
17.7	13.6
13.6	10.5
10.5	8.2
8.2	6.4
6.4	5.0
5.0	3.9
3.9	3.0
3.0	2.4
2.4	1.9
1.9	1.5
1.5	1.2

Using the midpoint value of these classes to represent r_i may lead to problems in resolution and so each of the 15 terms in Eq. (5) was subdivided into a number of equally spaced subsize classes and the midpoint of each of these small size ranges was used to calculate r_i. It was assumed that the distribution by weight with in any full class was constant. In these calculations corrections were introduced to compensate for the change in wavelength of the light when traversing the liquid, and for the effect of refraction when the scattered light is leaving the measuring cell.

Table 3: Scattering matrix as used by Malvern for a 63 mm lens and size intervals as listed in Table 2.

7.11E-03	6.60E-03	4.90E-03	3.71E-03	2.99E-03	2.28E-03	1.72E-03	1.31E-03
2.76E-03	7.83E-03	7.56E-03	6.25E-03	5.25E-03	4.08E-03	3.12E-03	2.40E-03
7.88E-04	5.98E-03	9.31E-03	8.99E-03	8.11E-03	6.53E-03	5.09E-03	3.96E-03
5.24E-04	2.57E-03	9.12E-03	1.14E-02	1.16E-02	9.89E-03	7.97E-03	6.32E-03
5.68E-04	8.77E-04	6.33E-03	1.27E-02	1.56E-02	1.47E-02	1.24E-02	1.02E-02
4.03E-04	1.26E-03	2.18E-03	1.04E-02	1.82E-02	2.01E-02	1.85E-02	1.59E-02
3.91E-04	1.25E-03	1.31E-03	4.70E-03	1.66E-02	2.44E-02	2.60E-02	2.42E-02
3.15E-04	1.06E-03	2.74E-03	1.38E-03	8.82E-03	2.25E-02	3.11E-02	3.32E-02
3.22E-04	1.09E-03	1.91E-03	4.09E-03	2.53E-03	1.29E-02	2.38E-02	3.87E-02
3.75E-04	9.56E-04	2.25E-03	3.65E-03	4.93E-03	5.12E-03	1.63E-02	3.41E-02
4.75E-04	1.11E-03	1.97E-03	3.85E-03	4.75E-03	8.53E-03	7.69E-03	1.74E-02
6.49E-04	1.39E-03	2.54E-03	3.40E-03	6.30E-03	7.50E-03	1.50E-02	5.19E-03
8.88E-04	1.84E-03	2.94E-03	4.81E-03	7.36E-03	7.78E-03	1.75E-02	1.25E-02
1.20E-03	2.41E-03	3.93E-03	5.81E-03	8.40E-03	1.12E-02	1.43E-02	2.01E-02
1.56E-03	3.08E-03	4.83E-03	6.57E-03	9.61E-03	1.54E-02	1.18E-02	2.81E-02
1.42E-03	9.04E-04	3.89E-04	9.98E-04	1.50E-03	1.24E-03	7.28E-04	1.34E-04
2.61E-03	1.66E-03	7.16E-04	1.84E-03	2.77E-03	2.29E-03	1.34E-03	2.47E-04
4.35E-03	2.78E-03	1.20E-03	3.09E-03	4.65E-03	3.86E-03	2.26E-03	4.16E-04
7.04E-03	4.35E-03	1.95E-03	5.06E-03	7.64E-03	6.34E-03	3.72E-03	6.85E-04
1.16E-02	7.51E-03	3.25E-03	8.49E-03	1.28E-02	1.07E-02	6.27E-03	1.16E-03
1.88E-02	1.24E-02	5.39E-03	1.42E-02	2.16E-02	1.80E-02	1.06E-02	1.96E-03
3.03E-02	2.05E-02	9.00E-03	2.42E-02	3.70E-02	3.10E-02	1.83E-02	3.39E-03
4.60E-02	3.26E-02	1.45E-02	4.00E-02	6.21E-02	5.24E-02	3.11E-02	5.79E-03
6.40E-02	4.88E-02	2.21E-02	6.43E-02	1.02E-01	8.70E-02	5.20E-02	9.79E-03
7.78E-02	6.73E-02	3.13E-02	9.96E-02	1.64E-01	1.42E-01	8.60E-02	1.65E-02
7.47E-02	7.99E-02	3.88E-02	1.43E-01	2.49E-01	2.23E-01	1.38E-01	2.71E-02
5.13E-02	7.72E-02	3.94E-02	1.88E-01	3.61E-01	3.40E-01	2.16E-01	4.46E-02
2.85E-02	5.37E-02	2.79E-02	2.14E-01	4.82E-01	4.90E-01	3.29E-01	7.32E-02
3.63E-02	2.59E-02	1.23E-02	1.99E-01	5.76E-01	6.65E-01	4.82E-01	1.23E-01
4.67E-02	1.55E-02	2.01E-02	1.38E-01	5.81E-01	8.20E-01	6.76E-01	2.19E-01

Scattering patterns were measured for four different suspensions of spherical, nearly monosized polystyrene latices. The standard deviations of the size distributions of the particle samples, were all less than 0.03. The composition of these suspensions is listed in Table 4, together with the letter index by which they will now be indentified.

Table 4: Composition of the measured polystyrene latex suspensions.

reference index	mean diameter (microns)	continuous phase	ratio of refractive indices (m)
a	4.5	ethanol	1.16
b	4.5	glycerine	1.10
c	18.3	ethanol	1.16
d	18.3	glycerine	1.10

The normalized distributions of the light-energy as calculated from theory and as obtained by experiment, are depicted for the different suspensions in Figures 5 through 8. Normalization was achieved by dividing the light-energies by the primary maximum value which occurs. This maximum value was then set to 2047. The theoretical results were calculated assuming the refractive index of polystyrene to be equal to (1.58). For the continuous phase the refractive indices were those of ethanol (1.36) and glycerine (1.43) respectively.

The normalized distributions which follow for the Malvern scattering matrix are listed in Table 5.

Table 5: Normalized light energy distributions which are derived from the Malvern scattering matrix corresponding with the size of the measured suspensions.

	light energy	
ring number	size class 3.9-5.0 microns	size class 17.7-23.7 microns
1	23	598
2	43	1007
3	71	1449
4	116	1837
5	192	2047
6	318	1676
7	525	758
8	835	222
9	1250	659
10	1724	588
11	2047	621
12	1978	548
13	1376	775
14	664	936
15	397	1059

5 Discussion

Suspension a.

In Figure 5 the results of the theoretical calculations and experiments are shown. Deviations from the measured pattern are

not too serious for segments 1 through 12. The major difference between theory and experiment lies in the rapid decrease of the light-energy on the outer segments predicted by calculations based on FD, and the more slower decrease as actually observed. These corresponding values for one segment may differ by a factor of ten.

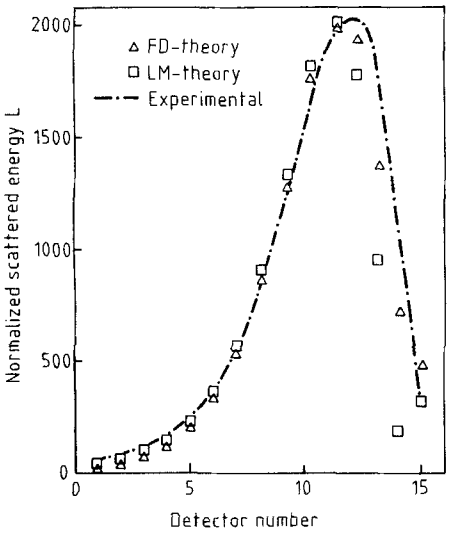

Fig. 5: Theoretical and experimental scattering patterns for suspension *a*.

This discrepancy between theory and experiment also exists for suspensions *b* through *d*.
The mean square deviation is defined by:

$$\sigma^2 = \frac{1}{15}\sum_{i=1}^{15}\{[L(i) - L_{cal}(i)]/L(i)\}^2 \qquad (9)$$

For the Fraunhofer approach it is equal to 0.30. The theoretical results based on Lorenz-Mie scattering agree very well with the experimental observations for segments 1 through 12. The theoretical predictions are considerably improved for the outer segments. The rapid decrease in light-energy, as calculated by FD, is not observed and the energy calculated for segment 15 is of the correct order of magnitude. For this case, the value of σ is equal to 0.26.
It must be borne in mind that the calculations apply to size-intervals, not to monosized particles.
In Table 5 the normalized light energy distributions as derived from the Malvern matrix are listed. Comparison of the data from the Malvern matrix with the experimental results yields $\sigma = 0.25$. The scattering pattern obtained from this matrix is almost identical to that as calculated using the Lorenz-Mie theory, even on detector segments 13, 14 and 15.

Suspension b.

The results are shown in Figure 6. The most striking difference between the distributions of light-energy for suspensions *a* and *b* is the amount of light striking the outer detector segments. Both the theoretical results based on FD and the pattern as derived from the Malvern matrix (see Table 5) show significant deviations from the light-energies actually measured. The values of the coefficient σ are 1.09 as obtained from the FD and 1.36 from the Malvern approaches respectively.

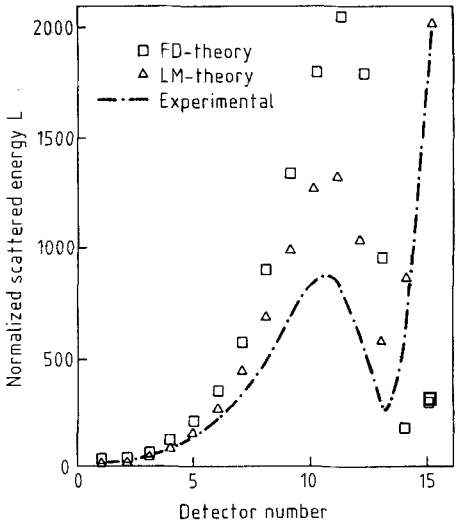

Fig. 6: Theoretical and experimental scattering patterns for suspension *b*.

Further it is observed that light-energies according to FD theory and the Malvern matrix decrease for detector segments 11 through 15. However, the light-energy falling onto segment 15 proves to be the maximum value that is measured.
Lorenz-Mie theory in contrast, predicts are correct behaviour, maximum light energy on segment 15. The main difference between this theory and the experimental results occur on detector segments 8 through 13. Those differences must be attributed to the fact that the data points are normalized with respect to the primary maximum of the scattering pattern. If the data points were normalised with respect to the secondary maximum (segment 11), it is easily shown that the results from experiment and Lorenz-Mie theory practically coincide for all the segments, except segment 15 where the lightenergy differs by 40 percent from the value which is actually observed. The value of σ is 0.45.

Suspensions c and d.

From Figures 7 and 8 it will be obvious that FD theory yields a poor prediction of the scattering patterns. Though the position of the primary maxima in these patterns agrees well with those

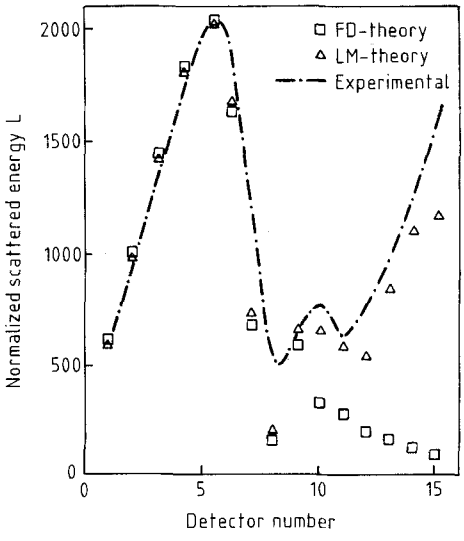

Fig. 7: Theoretical and experimental scattering patterns for suspension *c*.

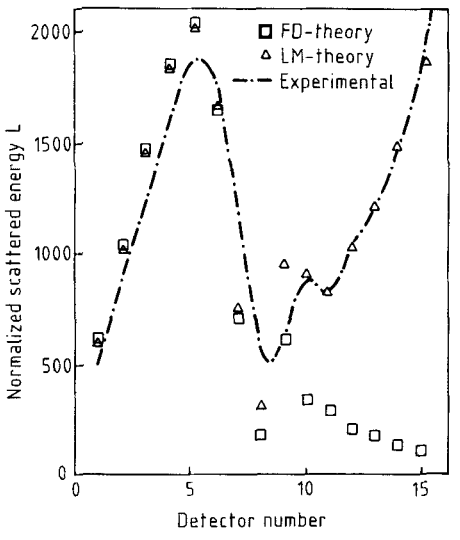

Fig. 8: Theoretical and experimental scattering patterns for suspension *d*.

which are experimentally observed, the theory does not explain the increasing values of the light-energy distributions on the outer detector segments. Lorenz-Mie theory, however, not only yields data points of the correct magnitude but also predicts the occurence of the three maxima on the energy distribution.

Scattering patterns as derived from the Malvern matrix (see Table 5) underestimate the light-energy falling on detector segments 12 through 15, particularly for suspension *d*. Lorenz-Mie theory is seen to yield almost perfect light-energy predictions for these segments.

It is also noticable that differences between the scattering patterns of suspensions *a* and *b* are more pronounced than those for suspensions *c* and *d*. This must be attributed to the difference in size of the particles which are present in the suspensions. As the particles become larger, the effect of the refractive index of the continuous phase on the scattering pattern tends to become less.

6 Conclusions

From the experimental and theoretical results obtained in this study, it must be concluded that the measurement of the size of particles suspended in a liquid medium using LDS is best described by Lorenz-Mie theory rather than by FD.

Using this theory, scattering matrices may be calculated. This may be useful for those cases in which calibration of the apparatus by standard materials is difficult, or simply as a check on calibrated matrices. To some extent, it also offers the possibility of extending the size-class limits of the weight-distribution.

7 Symbols and Abbreviations

$a(ij)$	element of scattering matrix A; row i, column j
$\underline{\underline{A}}$	scattering matrix
c	constant appearing in Eq. (1)
c_i	constant appearing in Eq. (4), equal to $a(ji)$ for detector-ring j
F	focal length of lens
I	light intensity in detection plane
I_0	light intensity in centre of detection plane
J_0	Bessel function: 0^{th} order, and 1^{st} kind
J_1	idem: 1^{st} order, and 1^{st} kind
K	constant appearing in Eq. (4)
$L_{s1,s2}$	light energy falling between two radii, s_1 and s_2, in the detection plane
m	ratio of refractive indices
M	number of size-classes number of detector rings
Q	error function; defined in Eq. (7)
R	particle radius
S	radial distance in the detection plane measured from the optical axis
W	$W(i)$: weight class i W_i: weight particle falling within size class i
x	size parameter $= 2\pi rs/\lambda F$
λ	wavelength of light
ρ	density of particles

8 References

[1] *M. Kerker:* The Scattering of Light and other Electromagnetic Radiation. Academic Press, New York 1969.

[2] *E. D. Hirleman, V. Oechsk, N. A. Chigier:* Response characteristics of laser diffraction particle size analysers: optical sample volume extent and lens effects. Opt. Eng. *23* (1984) 610-619.

[3] *M. Heuer, K. Leschonski:* Erfahrungen mit einem neuen Gerät zur Messung von Partikelgrößenverteilungen aus Beugungsspektren. Preprints Third Europ. Symp. Particle Characterization, Nürnberg (1984) 515-537.

[4] *A. Bürkholz, R. Polke:* Laser Diffraction Spectrometers/Experience in Particle Size Analysis. Part. Charact. *1* (1984) 153-160.

[5] *D. J. Brown, P. G. Felton:* Direct measurement of concentration and size for particles of different shapes using laser light diffraction. Chem. Eng. Res. Des. *63* (1985) 125-132.

[6] *B. B. Weiner:* Particle and droplet sizing using Fraunhofer diffraction. Chem. Anal. *73* (1984) 135-172.

[7] *J. Swithenbank, J. M. Beer, D. S. Taylor, D. Abbot, G. C. McCreath:* Experimental Diagnostics in Gas-Phase Combustion Systems. A Laser Diagnostic Technique for the Measurement of Droplet and Particle Size Distribution, in *B. T. Zinn* (ed.): Prog. Astronaut. Aeronaut., Vol. *53* (1977).

[8] *F. H. W. Mannens:* Internal report no. R497S. Department of Physics. Eindhoven University of Technology, 1981.